Chapter 5

Fabrication of Dye Sensitized Solar Cell and Its Characterization

5.1. Fabrication of Dye Sensitized Solar Cell and its characterization

The focus of this work is to explore the performance of photo anode materials in increasing the power conversion efficiency of dye sensitized solar cells by minimizing the recombination rate using barrier layer between photoelectrode and dye, as recombination is a problem that exists in DSSC and causes a loss of photogenerated electrons **[1].**

ZnO, TiO_2, CeO_2, CdS, CuO, and ZrO_2 were synthesized for being used as photoanode and barrier layers. Another set of materials namely TiO_2, TiO_2- ZrO_2 and Eu doped TiO_2-ZrO_2 was synthesized for being used as photoanode. Cells with layer of either single material or multiple layers of different materials were prepared, using glass as substrate. The placement of the layers was based on the energy level values of their Lowest Unoccupied Molecular Orbital (LUMO) **[2].** The layers were applied by the "Doctor Blade" method, to keep it simple, less time consuming and cost effective **[3-4].**

Preparation of Working electrode:

Fluorine doped Tin Oxide (FTO) coated glass substrate with surface resistivity of 15 Ω/sq. transmittance 80% and 2.2mm thickness were purchased from TECHINSTRO INSTRUMENTS, to be used as the base for photoanode, which is also called simply anode or working electrode. Single or multiple layers of different materials, as mentioned above, was coated on the anode.

The synthesized samples of ZnO, TiO_2, CeO_2, CdS, CuO, ZrO_2, TiO_2- ZrO_2 and Eu doped TiO_2-ZrO_2obtained as powders were further grinded in an agate mortar pastel with dilute acetic acid for one hour to prepare a paste. Triton X 100 was added to make the paste uniform and well dispersed. This paste was coated on the FTO coated glass substrate using doctor blade technique to make a layer. 3M scotch tape was used as a spacer to fix the size of applied layer at 1.2 cm X 1.2 cm. The film was dried in air at room temperature and then sintered for 30 min at 450° C.

Dye Fixation on Working Electrode:

Ruthenium based synthetic dye is most efficient and widely used for DSSC application as it has a high absorption coefficient across the solar spectrum. Apart from this, other synthetic dye like Rhodamine is also used. However, these dyes are costly. Hence, other alternatives need to be explored. One of the objectives of this work being cost effective and environment friendly approach, plant-based Anthocyanin dye, extracted from natural source pomegranate has been used as an alternative **[5-7]**. The working electrode was immersed in this dye for 18hours and kept in a dark place for the dye to be adsorbed on the surface of material properly. The electrode was then allowed to dry naturally and washed with isopropanol to remove the residual on-adsorbed dye.

Preparation of Electrolyte Solution:

Generally, the electrolyte solution contains I^-/I_3^- redox ions **[8]**, which provides the path for electron to flow from counter electrode to working electrode. In the present work, Potassium Iodide (KI) based electrolyte solution was prepared by dissolving 0.127 gm of Iodine (I_2) in 10 ml of Ethelyn Glycol solution. 0.83 gm of KI was mixed in above solution and stirred well for few minutes. The prepared solution was stored in a dark place to be used as electrolyte.

Preparation of Counter electrode:

Platinum is most efficient and commonly used counter electrode material but as it is expensive other alternatives need to be investigated **[9]**. One of the alternatives can be the use of carbon-based materials. However, it may lead to a decrease in the efficiency of DSSC. Graphite, graphene or carbon coated FTO is also used as a counter electrode. In the present work, a thin layer was coated on FTO using graphite pencil.

Assembling of DSSC:

The working and counter electrodes were fixed together to prepare the cell. A thin film of polyethylene was placed at the edges between the two electrodes to provide insulation between them. Both the electrodes were sandwiched together by binder clips. The electrolyte solution was introduced between two electrodes through capillary force. The fabrication assembly is shown in figure 1.

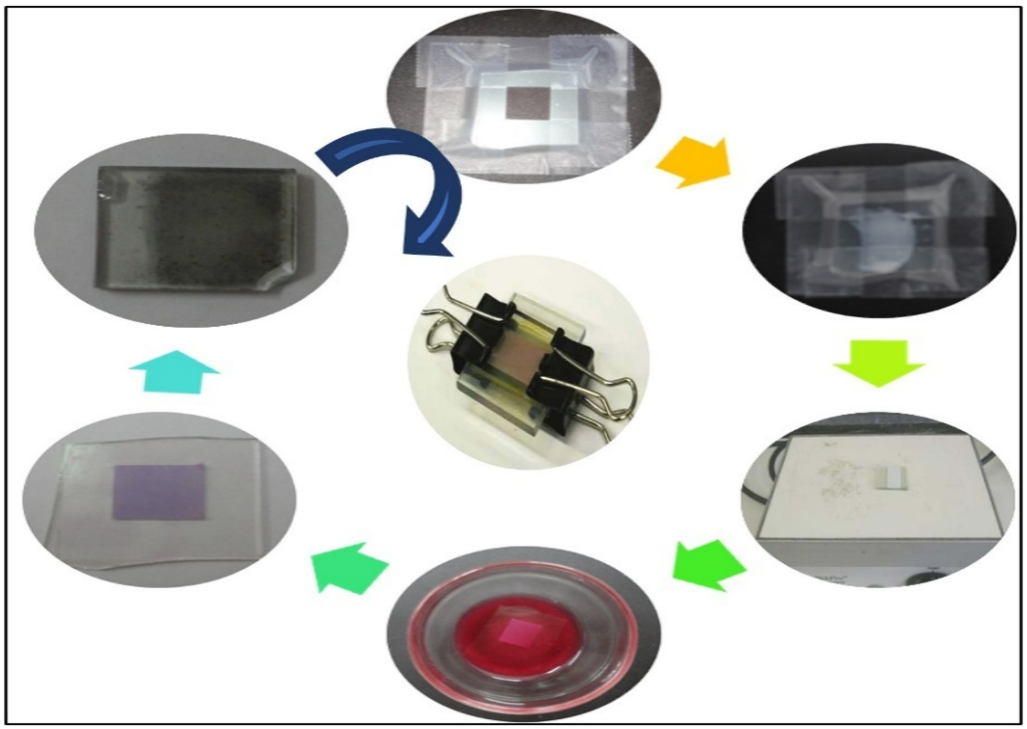

Figure 1: Fabrication process of dye sensitized solar cell.

The I-V characteristics of the cells were measured with a fixed load under illumination. For illumination, white LED bulb of 10 W was used. For measuring current and voltage, a Keithley source meter model 4200 was used. For these measurements, an assembly which can hold the solar cell with contact arrangements was prepared. The setup for efficiency measurements and contact arrangements are shown in figure 2.

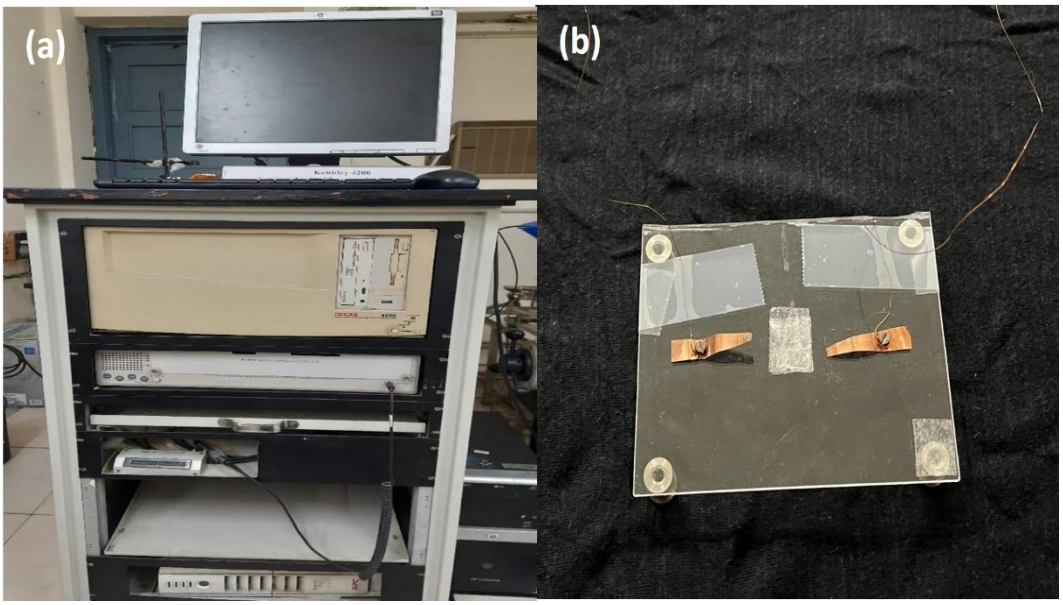

Figure 2: (a) I-V characteristic set up, (b) contact arrangement.

Parameters to be measured:

Short circuit current: $\mathbf{I_{SC} = I \quad (at\ V = 0)}$

For an ideal cell, I_{SC} is the maximum current or total current produced in the solar cell by photon excitation.

Open Circuit Voltage: $\mathbf{V_{OC} = V\ (at\ I = 0)}$

Open circuit voltage occurs when there is no current passing through the cell. V_{OC} is also the maximum voltage difference across the cell.

Maximum Power: $\mathbf{P_{max} = I_{max} \times V_{max}}$

Maximum power produced by cell can be calculated from I-V curve.

Power Density: $\mathbf{P = JV}$

The power density of the cell is given by the product of photocurrent density at short circuit ($J = I_{sc}$/surface area of the cell) and voltage (V).

Fill Factor: $\mathbf{FF = \frac{J_{max} \times V_{max}}{J_{SC} \times V_{OC}}}$

The fill factor is the ratio of the maximum obtainable power to theoretical power. When the fill factor value is close to 1, it can be considered as an efficient cell.

Power Conversion Efficiency: $\mathbf{\eta = \frac{J_{SC} \times V_{OC} \times FF}{P_{in}}}$

where P_{in} = Input power (power of light source)

5.2. Performance of Dye Sensitized Solar Cell fabricated using single layer of different material

Dye sensitized solar cell using the prepared material (ZnO, TiO_2, CeO_2, CdS, CuO and ZrO_2) were fabricated using the procedure mentioned above. The film was applied using doctor blade method. The significant parameters that affect the efficiency of DSSC like physiochemical and structural properties of material, porosity of the material, particle size of material, precise area, thickness and uniformity of the film are difficult to control during fabrication process. An attempt was made to maintain the uniformity of the paste by taking the same amount of material for grinding, maintaining the same time interval of grinding and using the same amount of surfactant for each cell. All other parameters like type of dye, dye adsorption time, amount of electrolyte solution, etc. was fixed.

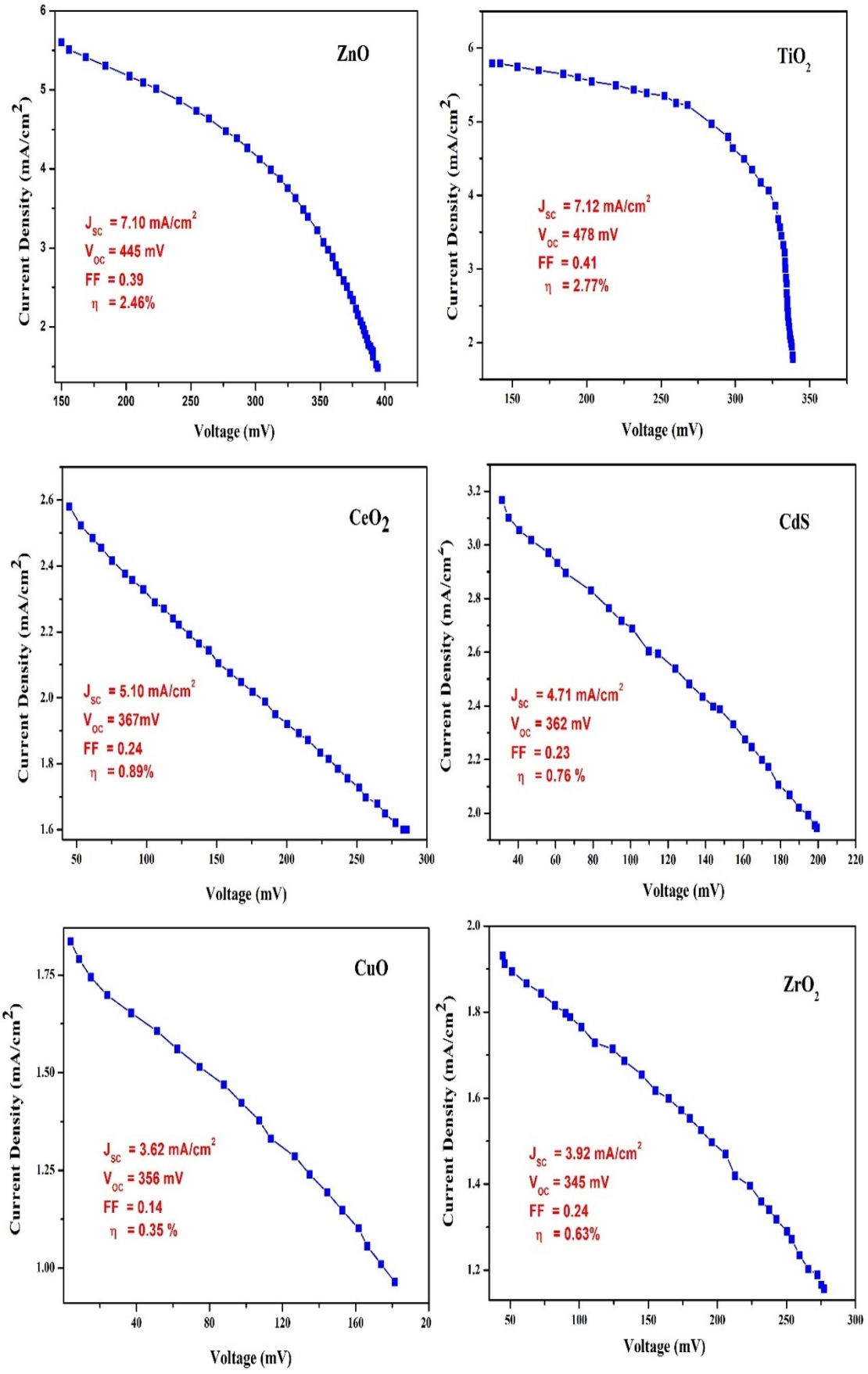

Figure 3. I-V curves of DSSC prepared using single layer.

Table 1: Efficiency parameters of DSSCs prepared using different material.

Sample	Thickness (μm)	Area Cm^2	J_{SC} mA/cm^2	V_{OC} V	FF	η %
ZnO	10.45	1.44	7.10	0.445	0.39	**2.46**
TiO_2	11.34	1.44	7.12	0.478	0.41	**2.77**
CeO_2	11.56	1.44	5.10	0.367	0.24	**0.89**
CdS	10.78	1.44	4.71	0.362	0.23	**0.76**
CuO	10.98	1.44	3.62	0.356	0.14	**0.35**
ZrO_2	11.34	1.44	3.92	0.345	0.24	**0.63**

I-V characteristic curves of fabricated cells having a single layer of different material are shown in Figure 3. Other parameters of the cells are given in Table 1. The efficiency of the DSSC can vary significantly depending on the specific materials used as photoelectrode. The table shows the efficiency of these cells varying from 0.35% to 2.77 %. Highest efficiency has been observed for the cell prepared with TiO_2 layer and lowest efficiency has been observed for CuO layer. This is a substantial variation which can be attributed to various factors including light absorption, electron transport, charge recombination and the performance of the dye.

ZnO and TiO_2 are widely used as active materials for solar cells due to their excellent electron transport properties and bandgap that allow for efficient electron injection from the dye to the active material **[10]**. In the present case, ZnO based cell exhibits slightly lower efficiency compared to TiO_2. It is significant to mention here that the crystallite size of ZnO at 23.94 nm is higher than that found for TiO_2, which is 12.68 nm. Smaller crystallite size can result into larger surface area facilitating a higher amount of dye loading capacity. This would consequently generate more photoelectrons **[11]**. The values of crystallite size are given in Chapter 4.

The I-V characteristic curves of cells also reflect and corroborate the better performance of cells with ZnO and TiO_2 layers as active materials. Both these cells exhibit good photovoltaic characteristics while the cells with single layer of CeO_2, CdS,

ZrO_2 and CuO show flat characteristics like ordinary resistance. This resistor like behaviour indicates poor generation of photoelectrons or inefficient transport of photogenerated electrons.

Cells prepared using single layers of CeO_2, CdS, ZrO_2 and CuO show poor efficiencies of less than 1%. Although their crystallite size is on the lower side, it has been reported in the literature that CeO_2, CdS, CuO and ZrO_2 have low dye loading capacity compared to ZnO and TiO_2 **[12,13]**. This points out to poor adsorption, which in turn would result into lower photoelectron production.

Efficient electron transport is crucial for the rapid transfer of charges to the electrode, thus minimizing recombination losses and producing a higher photocurrent. In the approach under consideration the LUMO levels of CeO_2, CdS, CuO and ZrO_2 are closer to the LUMO level of the dye compared to FTO plate as shown in figure 4. The photogenerated electrons switching from LUMO level of dye to material have a reasonable chance of recombination with the hole in LUMO level of dye or going back to the valence band of the active material before reaching the FTO layer of the working electrode. This would eventually reduce the efficiency of charge collection and lower the overall power conversion efficiency **[14]**. The recombination can be checked by introduction of barrier layers. This work attempts to explore the performance of cells with a single or multiple barrier layer.

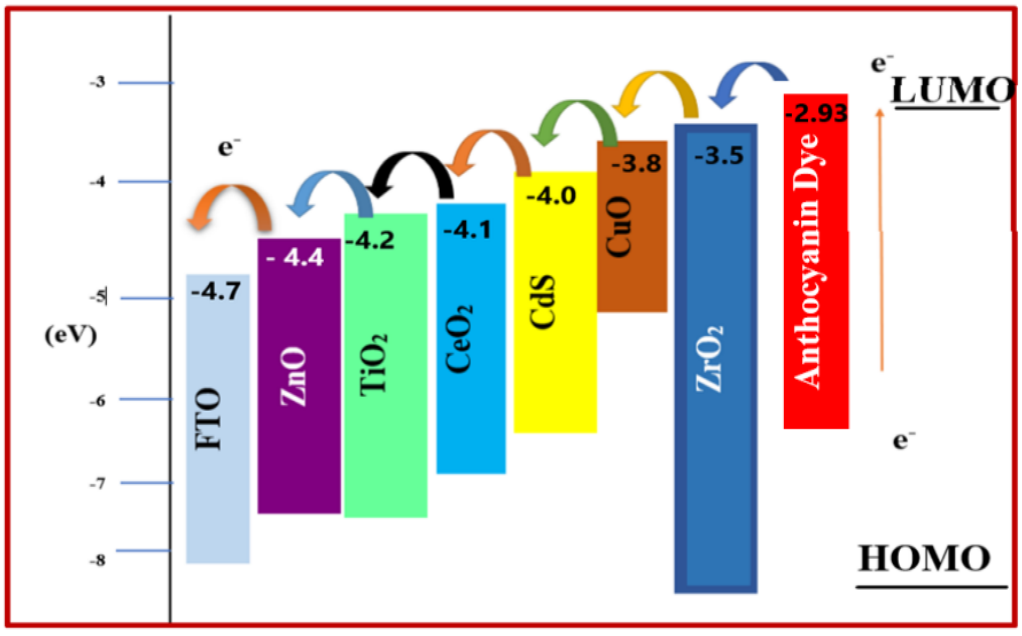

Figure 4: LUMO energy levels of different materials.

5.3. Performance of Dye Sensitized Solar Cell fabricated with two layers of different material (One as active material and other barrier layer)

As the purpose of present work is to increase the efficiency of DSSC by reducing recombination, a barrier layer of another material was deposited on working electrode. A comparison of energy levels of the synthesized materials makes it clear that ZnO has a LUMO level nearest to the FTO followed by TiO_2, CeO_2,CdS, CuO and ZrO_2 in that order **[12]**. Hence, a layer of ZnO was first deposited on the FTO substrate as active material, making it the part of the working electrode, which is common for all the cells. This was followed by applying a layer of another material to act as the barrier layer for inhibiting recombination. Four cells were prepared for each material of barrier layer with different thickness. The I – V characteristics of these cells were recorded.

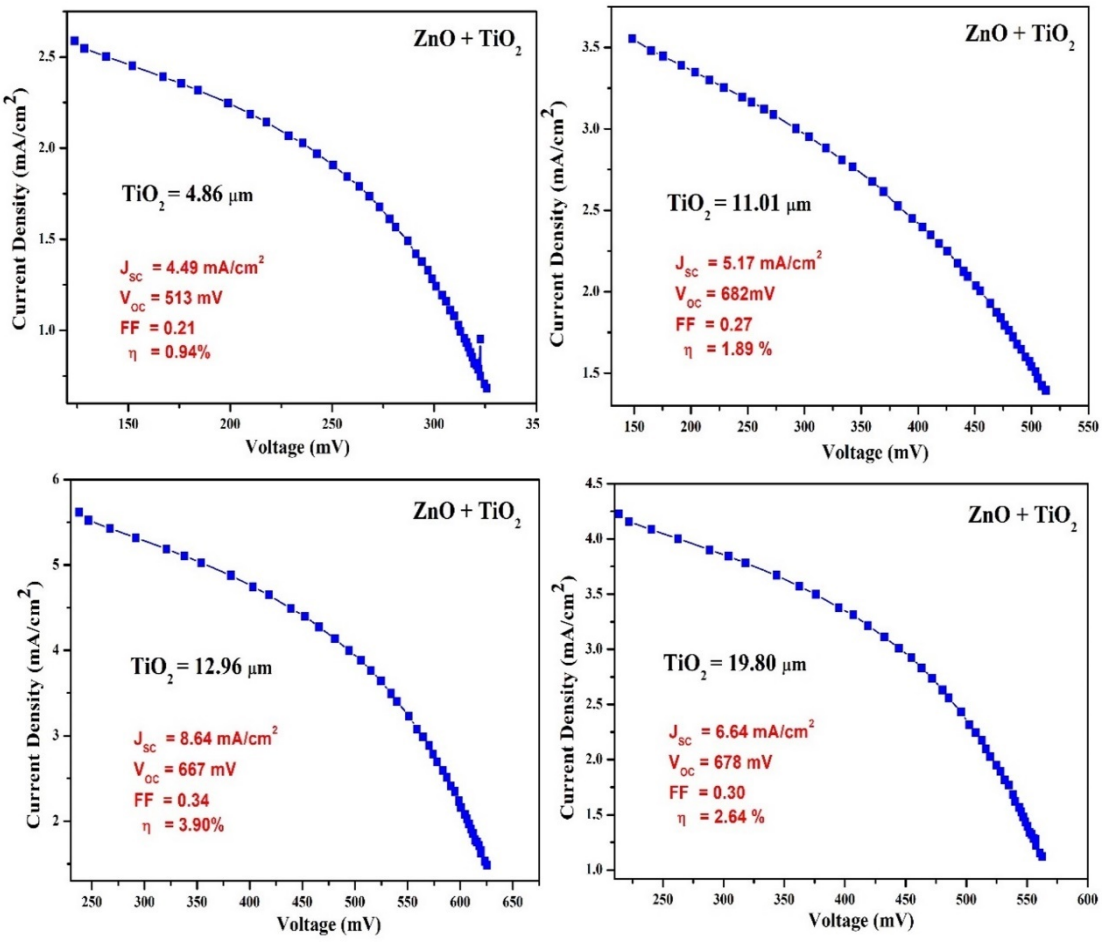

Figure 5. I-V curves of DSSC prepared using ZnO+TiO_2 layer.

Table 2: Efficiency parameters of DSSCs prepared using ZnO+TiO_2 electrode.

Sample	Thickness of ZnO	Thickness of TiO_2 (µm)	Area Cm^2	J_{SC} mA/cm^2	V_{OC} V	FF	η %
ZnO + TiO_2	~2.4 µm	4.86	1.44	4.49	0.513	0.21	**0.94**
		11.01	1.44	5.17	0.682	0.27	**1.89**
		12.96	1.44	8.64	0.667	0.34	**3.90**
		19.80	1.44	6.64	0.678	0.30	**2.64**

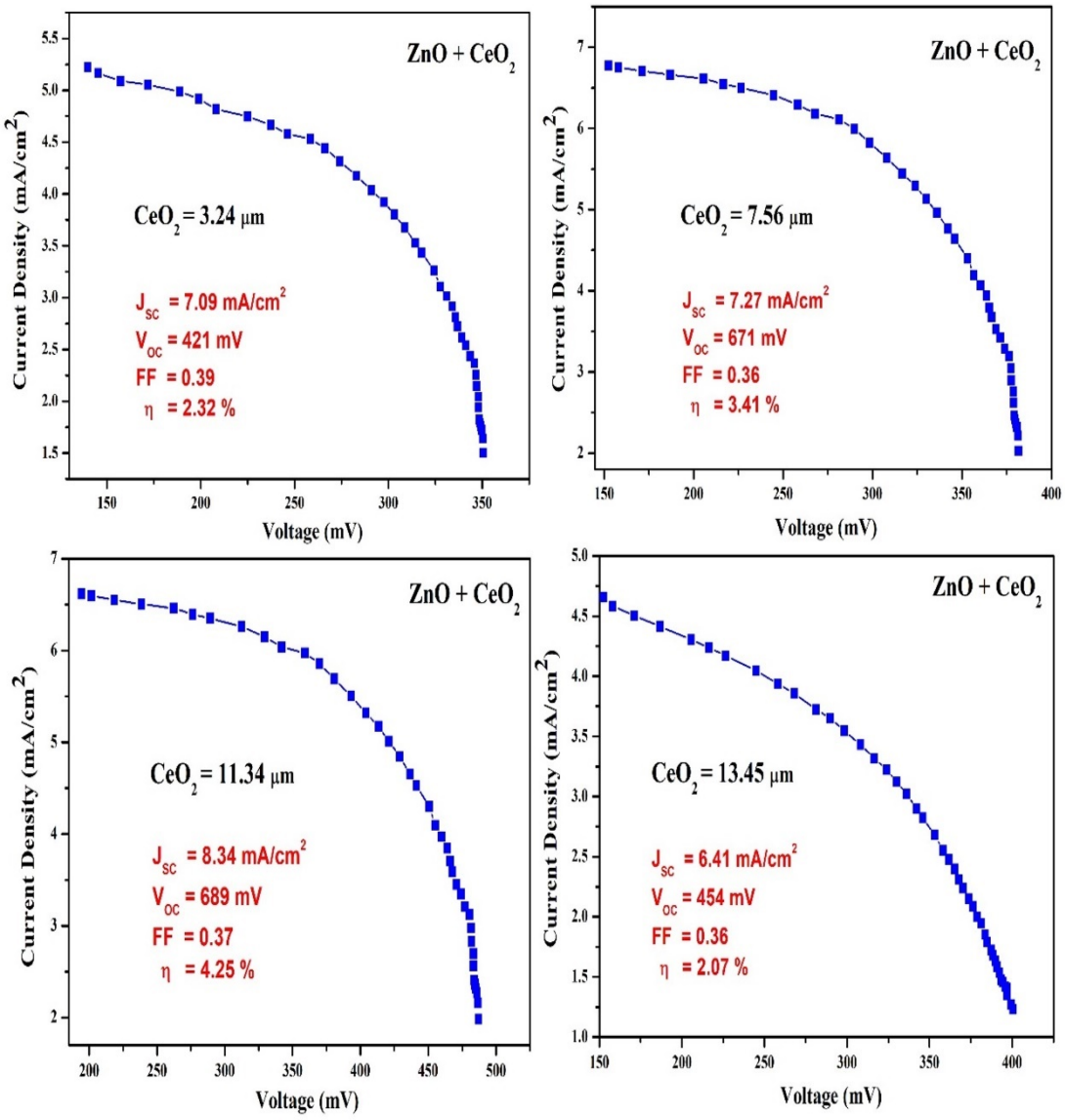

Figure 6. I-V curves of DSSC prepared using ZnO+CeO_2 double layer.

Table 3: Efficiency parameters of DSSCs prepared using ZnO+CeO_2electrode.

Sample	Thickness of ZnO	Thickness of CeO_2 (µm)	Area Cm^2	J_{SC} mA/cm^2	V_{OC} V	FF	η %
ZnO + CeO_2	~2.4 µm	3.24	1.44	7.09	0.421	0.39	**2.32**
		7.56	1.44	7.27	0.671	0.36	**3.41**
		11.34	1.44	8.34	0.689	0.37	**4.25**
		13.45	1.44	6.41	0.454	0.36	**2.07**

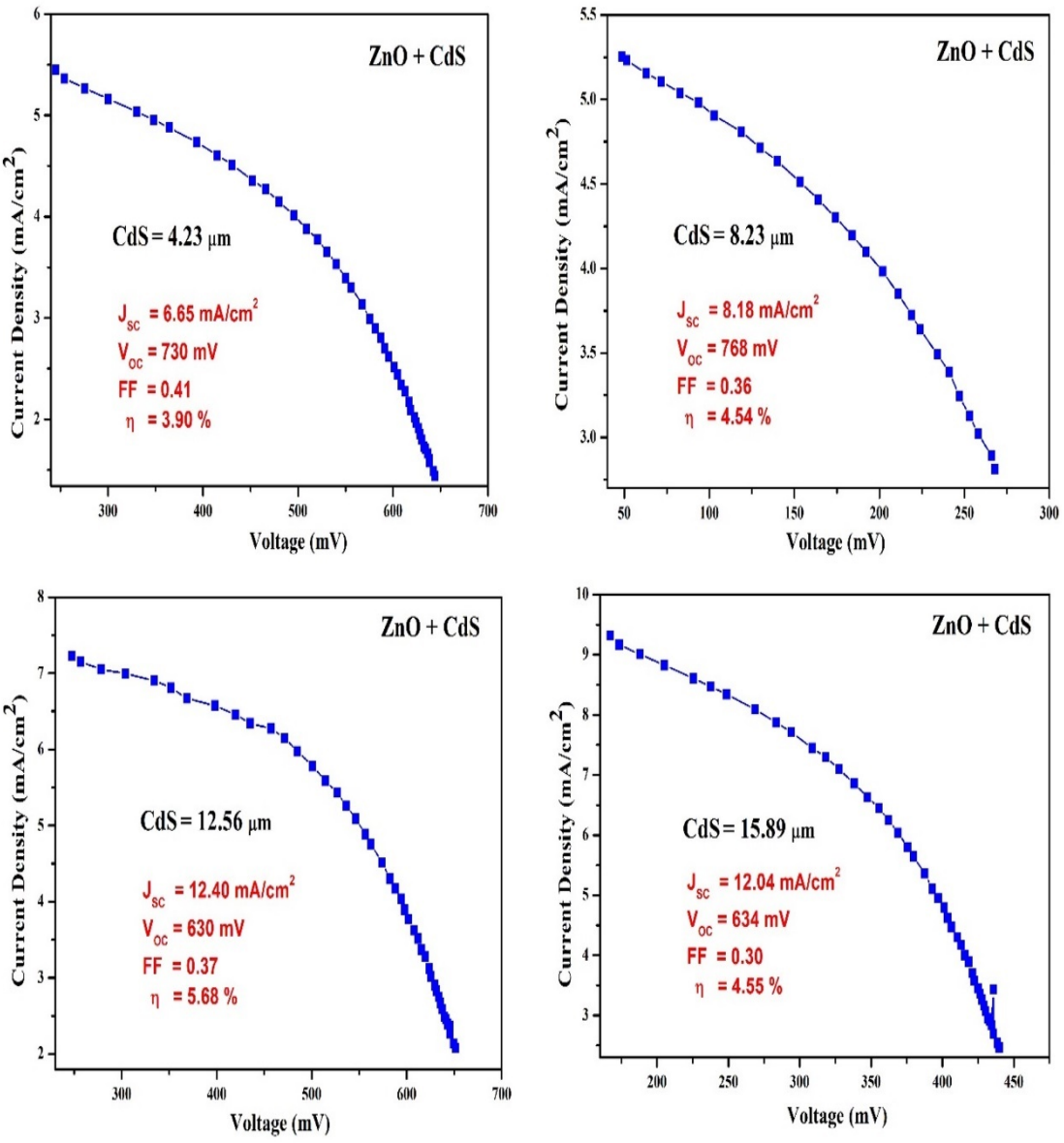

Figure 7. I-V curves of DSSC prepared using ZnO + CdS double layer.

Table 4: Efficiency parameters of DSSCs prepared using ZnO + CdS electrode.

Sample	Thickness of ZnO	Thickness of CdS(µm)	Area Cm^2	J_{SC} mA/cm^2	V_{OC} V	FF	η %
ZnO + CdS	~2.4 µm	4.23	1.44	6.65	0.73	0.41	**3.90**
		8.23	1.44	8.18	0.768	0.36	**4.54**
		12.56	1.44	12.40	0.630	0.37	**5.68**
		15.89	1.44	12.04	0.634	0.30	**4.55**

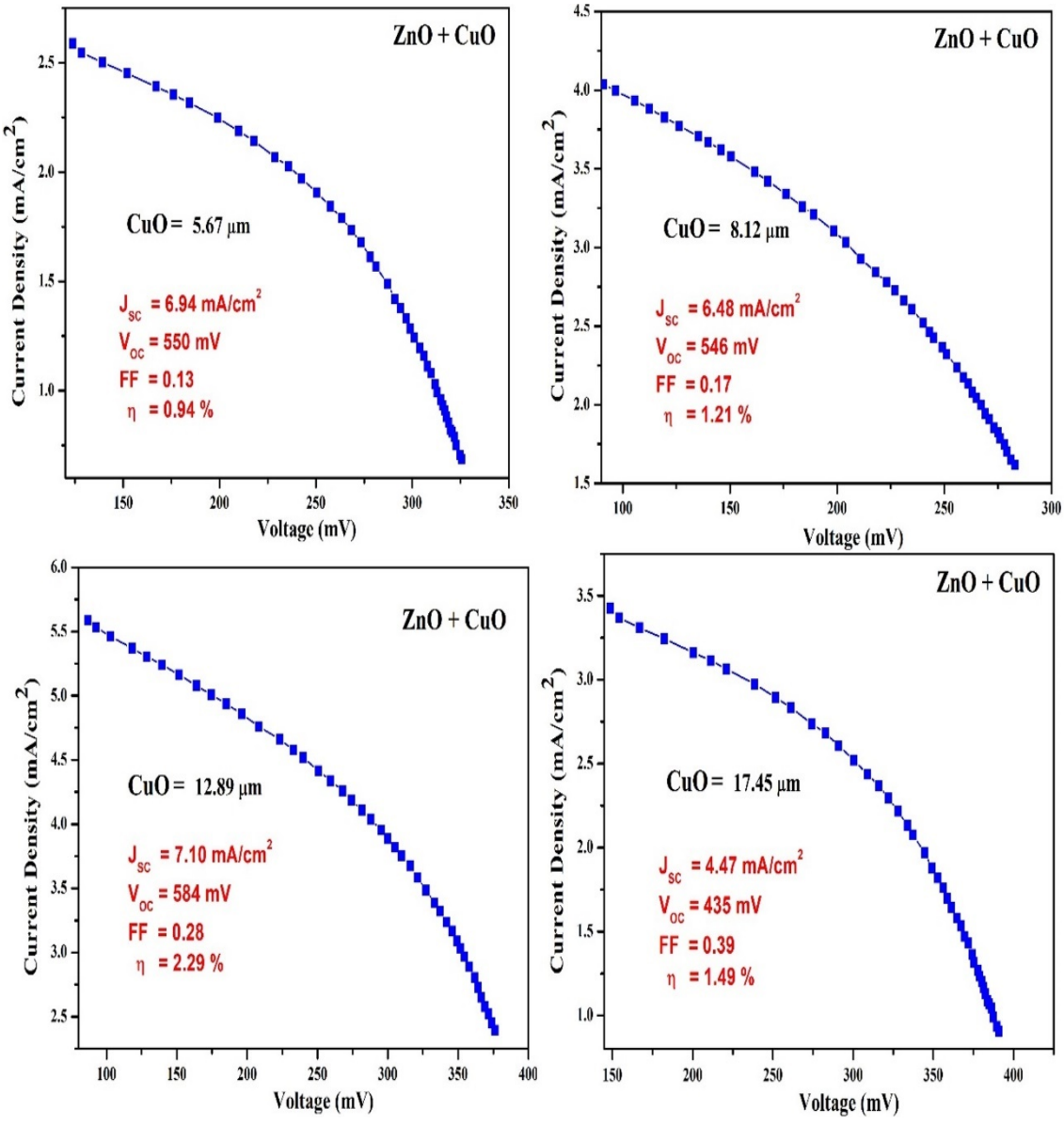

Figure 8. I-V curves of DSSC prepared using ZnO + CuO double layer.

Table 5: Efficiency parameters of DSSCs prepared using ZnO + CuO electrode.

Sample	Thickness of ZnO	Thickness of CuO(µm)	Area Cm^2	J_{SC} mA/cm^2	V_{OC} V	FF	η %
ZnO + CuO	~2.4 µm	5.67	1.44	6.94	0.550	0.13	**0.94**
		8.12	1.44	6.48	0.546	0.17	**1.21**
		12.89	1.44	7.10	0.584	0.28	**2.29**
		17.45	1.44	4.47	0.435	0.39	**1.49**

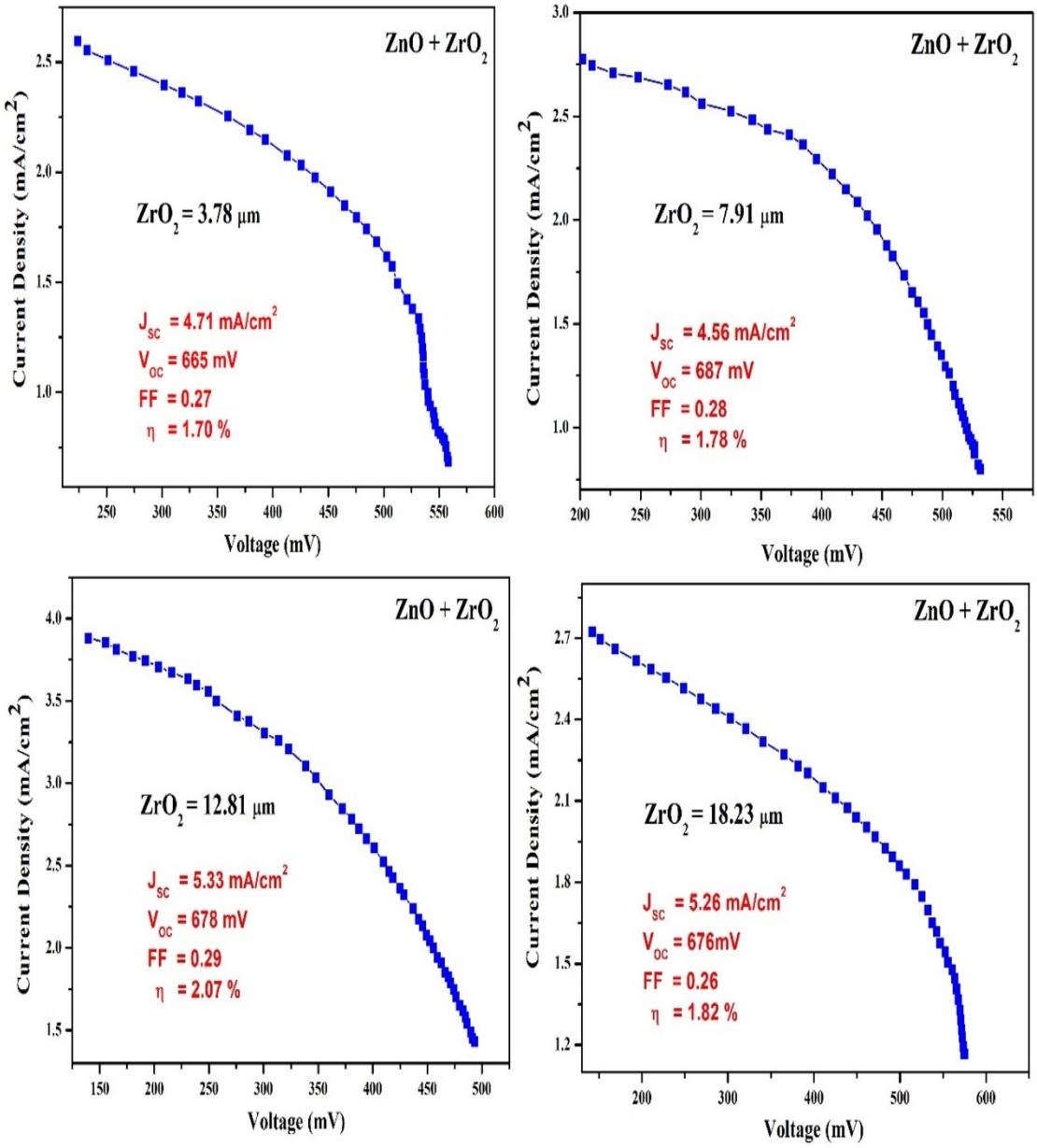

Figure 9. I-V curves of DSSC prepared using ZnO + ZrO_2 double layer.

Table 6: Efficiency parameters of DSSCs prepared using ZnO + ZrO_2electrode.

Sample	Thickness of ZnO	Thickness of ZrO_2(µm)	Area Cm^2	J_{SC} mA/cm^2	V_{OC} V	FF	η %
ZnO + ZrO_2	~2.4 µm	3.78	1.44	4.71	0.665	0.27	**1.70**
		7.91	1.44	4.56	0.687	0.28	**1.78**
		12.81	1.44	5.33	0.678	0.29	**2.07**
		18.23	1.44	5.26	0.676	0.26	**1.82**

The I-V characteristic curves of each of these set of cells are given in Figures 5 to 9, while Tables 2 to 6 enlist their efficiency parameters. The variation in efficiency of the cells with thickness of the barrier layer can be seen in the tables. The maximum efficiency of the sets varies from **2.07%** for ZnO + ZrO_2combination to **5.68 %**for ZnO + CdS combination**.**

Notably, the highest efficiency recoded is **5.68%**, for DSSC prepared with ZnO and CdS. The efficiency of DSSCs is influenced by multiple factors, among which the materials employed in their construction play a crucial role. TiO_2, CeO_2, CdS, ZrO_2, CuO and ZnO are commonly explored materials in DSSCs, and their combined use can positively impact the overall efficiency [**15, 16]**. Utilizing two layers in a DSSC yields higher efficiency compared to using a single layer material alone.

Layers with different material have different transport properties. Combining these materials and creating heterojunction between them, can facilitate more efficient electron transfer **[17]**. This reduces the chances of charge recombination, where electron and holes recombine before reaching the external circuit. As shown in the figure 4, the alignment of energy levels between conduction band and valence band between different materials leads to a gradient which can result into effective charge separation and transport.

The crystallite size of the material used for bi-layer coating of photoelectrode plays a significant role in influencing the efficiency of Dye-Sensitized Solar Cells

(DSSCs) **[18]**. The average crystallite size of materials used is between 23.94 nm and 12.68 nm. Particle size of two different layers deposited on photoelectrode is different than each other but still in nanometres. Smaller crystallites typically provide a larger surface area. This increased surface area enhances the contact interface between the semiconductor material and the dye molecules, promoting more efficient dye absorption and consequently better light absorption. Smaller crystallites can also provide better penetration into the porous structure of the electrode, ensuring a more intimate contact between the semiconductor material and the conducting substrate**[19]**. This improved contact can enhance charge collection efficiency. Besides, the different crystallite size can lead to a more efficient packing structure within the semiconductor layer. This optimized packing can improve electron percolation pathways and reduce the likelihood of charge carriers getting trapped **[20, 21]**.

The refractive index of prepared material lies in the range from 2.03 to 3.04, which is on the higher side. High refractive index materials can extend the path length of photons within the semiconductor layer **[22]**. This prolonged interaction between light and the semiconductor increases the likelihood of photon absorption, leading to a more efficient utilization of sunlight for energy conversion. Hence, higher refractive index can lead to improved efficiency of DSSC.

The cells prepared using ZnO + ZrO_2 and ZnO + CuO combinations show very less efficiency than the cells prepared using single ZnO layer **[23]**. This might be due the alignment of energy levels. As shown in figure 4 the conduction band of dye, ZrO_2 and CuO are very close to each other compare to ZnO **[12]**. Hence, there is a higher chance of excited electrons to recombine from conduction band of dye to the valence band of dye, ZrO_2 or CuO, rather than moving to ZnO and FTO.

5.4. Performance of Dye Sensitized Solar Cell fabricated with three layers of different material (One as active material and two barrier layers)

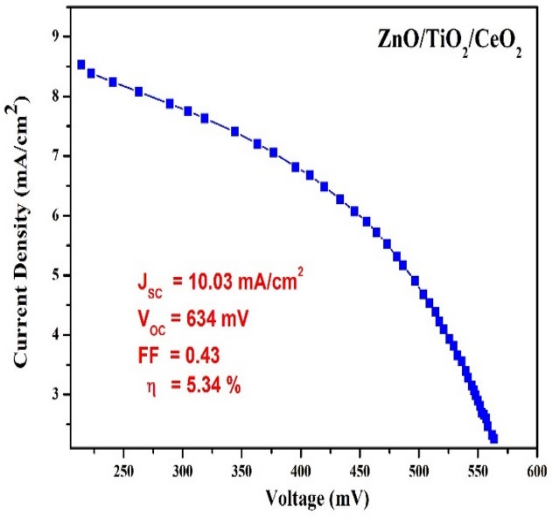

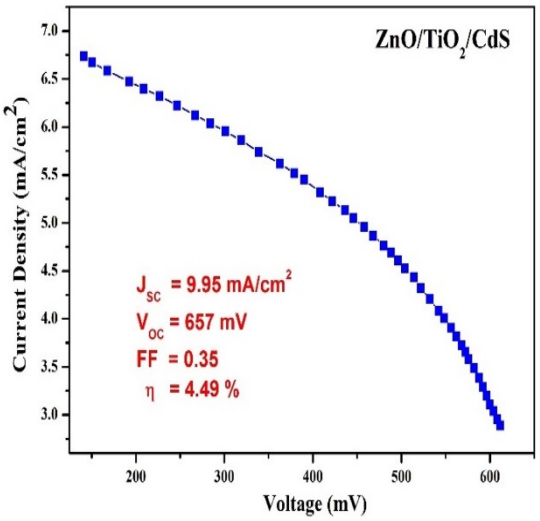

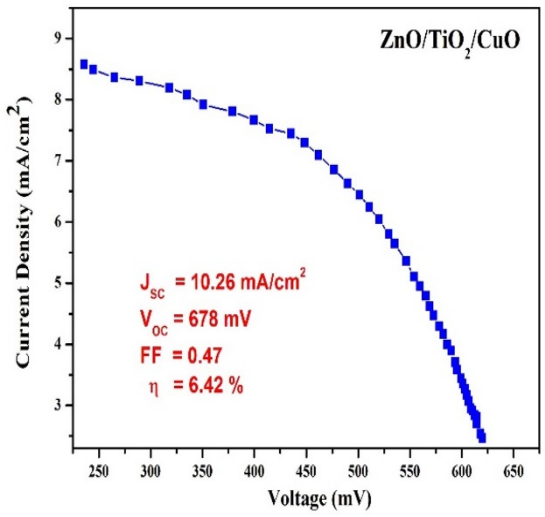

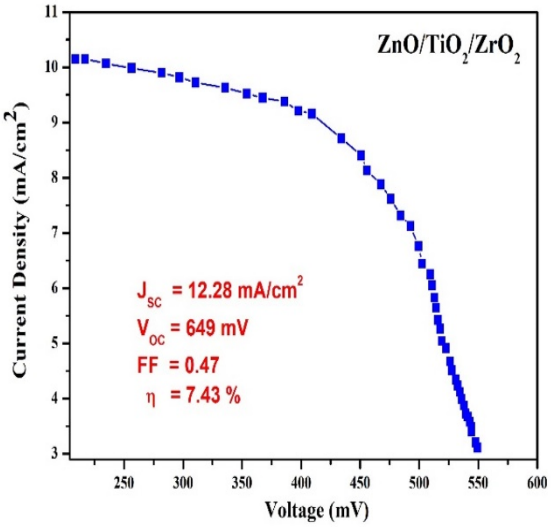

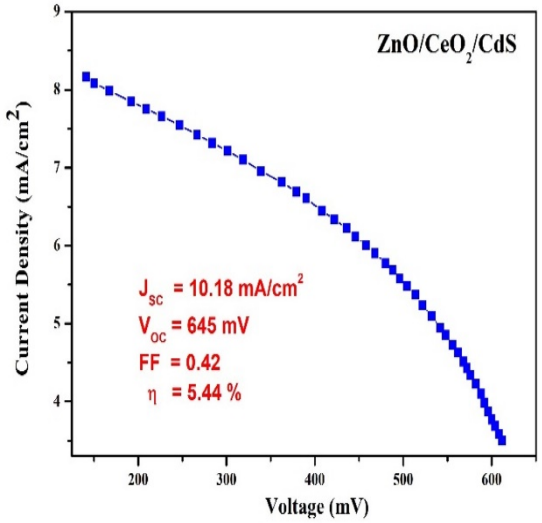

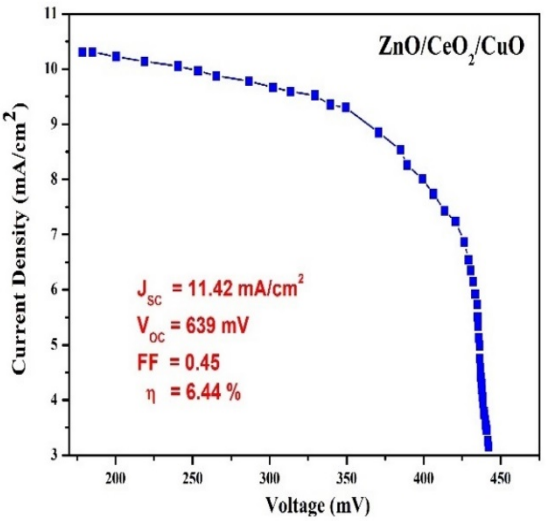

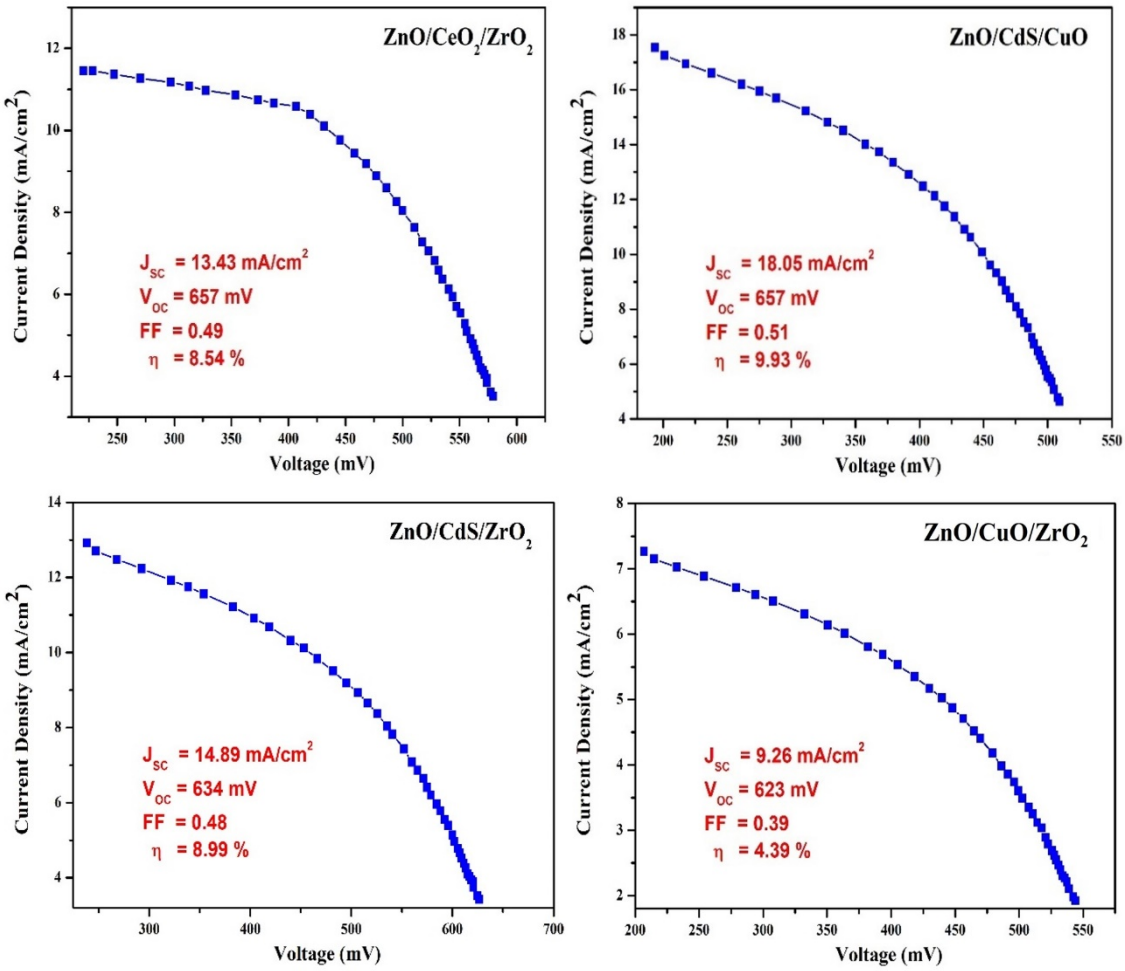

Figure 10. I-V curves of DSSC prepared using three different layers.

Since, utilizing two layers in a DSSC yields higher efficiency compared to using a single layer material alone, it is logical to explore the performance of DSSC with three layers, one as active material and two as barrier layers with varying LUMO energy levels **[24-26]**. The dual layers were deposited onto the ZnO-coated electrode, with their selection based on the LUMO energy levels depicted in Figure 4.The combined thickness of the three coating layers was kept at approximately 12 µm, a value determined to be optimal based on earlier investigations of cells fabricated for the study. In total 10 solar cells with different combinations were prepared and their I-V characteristics were studied.

Figure 10 shows the I-V characteristics of prepared cells. The photovoltaic properties are given in table 7. The nature of I-V curves show good photovoltaic characteristics. It is visible that the efficiencies of the cells increased on incorporation of the additional barrier layer.

Table 7: Efficiency parameters of DSSCs prepared using three different layers.

Samples	Thickness (µm)	Area Cm^2	J_{SC} mA/cm^2	V_{OC} V	FF	η %
ZnO / TiO_2/ CeO_2	11.89	1.44	10.03472	0.634	0.42817	**5.34**
ZnO / TiO_2 /CdS	12.13	1.44	9.95833	0.657	0.34977	**4.49**
ZnO / TiO_2 / CuO	11.98	1.44	10.26389	0.678	0.47052	**6.42**
ZnO / TiO_2 / ZrO_2	12.78	1.44	12.27778	0.649	0.47547	**7.43**
ZnO / CeO_2/ CdS	12.89	1.44	10.1875	0.645	0.42213	**5.44**
ZnO / CeO_2/ CuO	12.45	1.44	11.42361	0.639	0.45005	**6.44**
ZnO / CeO_2/ ZrO_2	11.67	1.44	13.43056	0.657	0.49357	**8.54**
ZnO / CdS / CuO	**12.24**	1.44	**18.05**	**0.657**	**0.51**	**9.93**
ZnO / CdS / ZrO_2	12.01	1.44	14.89	0.634	0.48564	**8.99**
ZnO / CuO/ ZrO_2	13.45	1.44	9.26	0.623	0.39	**4.39**

The Dye-Sensitized Solar Cell (DSSC) with a ZnO/CdS/CuO photoelectrode exhibited the highest efficiency at **9.93%,** while the lowest efficiency of **4.39%** was observed for the DSSC with a ZnO/ZrO_2/CuO photoelectrode. The enhancement in efficiency can be attributed to the introduction of two barriers that effectively inhibit recombination**[27]**. Proper alignment of energy bands between adjacent layers is crucial for efficient charge transfer and reduced recombination. As mentioned in the energy band diagram (figure 4), the conduction band alignment of CuO, CdS and ZnO forms a step-like nature. This step-like configuration facilitates a gradient, which leads to smooth and rapid transfer of electrons, further inhibiting recombination and promoting efficient charge transport. This can result in improved charge carrier mobility, reducing the chances of recombination and enhancing the overall efficiency of electron collection **[28]**.

As the bandgap of material used for tri layer coating covers a wide range in the solar spectrum, it likely provides a broader absorption range **[29, 30]**. This allows for better utilization of a wider range of solar wavelengths, leading to increased light absorption and consequently improves efficiency.

5.5. Performance of Dye Sensitized Solar Cell fabricated with Multi- layer of different materials (One as active material and rest barrier layers)

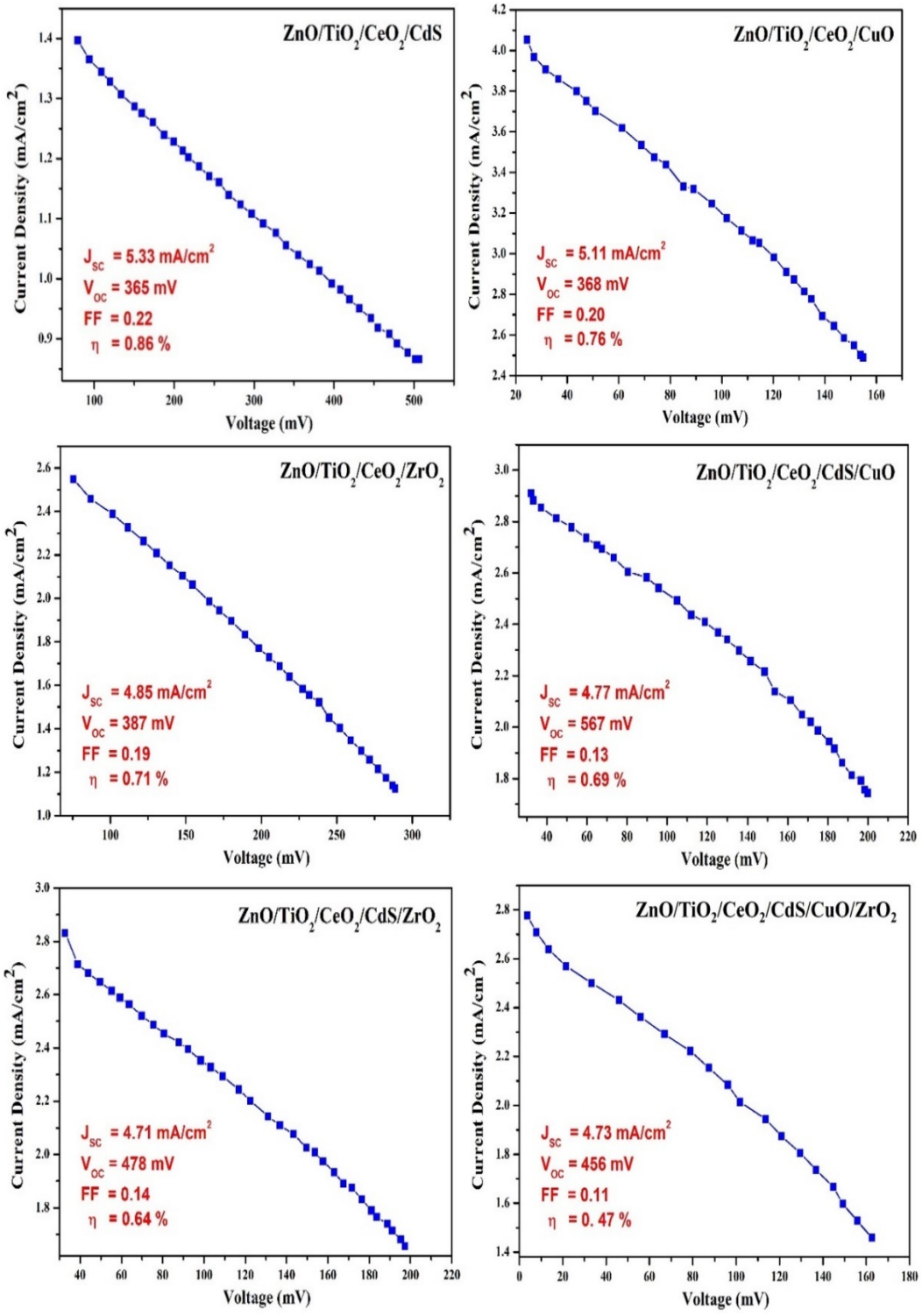

Figure 11. I-V curves of DSSC prepared using multi-layered electrode

Table 8: Efficiency parameters of DSSCs prepared using multi-layered electrode

Sample	Thickness (µm)	Area Cm^2	J_{SC} mA/cm^2	V_{OC} V	FF	η %
ZnO / TiO_2 / CeO_2 / CdS	18.23	1.44	5.33	0.365	0.225	**0.86**
ZnO / TiO_2 / CeO_2 / CuO	19.67	1.44	5.11	0.368	0.20	**0.76**
ZnO / TiO_2 / CeO_2 / ZrO_2	19.45	1.44	4.85	0.387	0.19	**0.71**
ZnO / TiO_2 / CeO_2 / CdS / CuO	22.56	1.44	4.77	0.567	0.13	**0.69**
ZnO / TiO_2 / CeO_2 / CdS / ZrO_2	22.13	1.44	4.71	0.478	0.14	**0.64**
ZnO / TiO_2 / CeO_2 / CdS / CuO/ ZrO_2	23.45	1.44	4.73	0.456	0.11	**0.47**

The utilization of a tri-layered approach in DSSC enhanced its performance. This suggests the effectiveness of barrier layers in enhancing the efficiency, the most likely reason for which is the inhibition of the recombination process. Consequently and logically, an effort was undertaken to fabricate a multi-layered photoelectrode for DSSC, with subsequent analysis of its efficiency parameters **[31]**. The choice of the depositing layer on the ZnO electrode was determined by arranging materials in ascending order of their LUMO energy levels. This arrangement creates a step-like structure, facilitating a pathway for the electron transport process, utilizing the LUMO gradient.

Figure 11 illustrates the I-V curves for cells fabricated using multiple barrier layers. The curves exhibit a resistor-like nature, indicating a higher resistance within the cells and therefore, a reduced generation of photocurrent. This observation is consistent with the parameters given in Table 8, which show a significant decrease in efficiency. As the film thickness increases due to the addition of extra layers, the efficiency declines. The increased film thickness may lead to electrons being trapped within the film, impeding their journey to the conducting plate. The higher film thickness introduces elevated resistance, hindering the flow of electrons **[32]**. The highest efficiency observed for multi-layered DSSC is **0.86 %**.

Adding multiple layers to the structure can introduce additional interfaces between materials. These interfaces may result in increased resistance and can hinder the efficient flow of electrons, leading to losses and decreased overall efficiency. The presence of multiple interfaces may provide additional centres for electron-hole

recombination. If the interfaces are not well-engineered to minimize recombination, it can result in a decrease in the number of electrons reaching the external circuit. The introduction of multiple layers often adds thickness to the electrode. While some layers may contribute positively to charge separation and transport, excessive thickness can lead to longer diffusion lengths for charge carriers, potentially increasing recombination losses as well as increasing the resistive path. The fabrication process for multilayer electrodes can be complex, and achieving uniformity and quality across all layers is challenging. Inconsistencies or defects in the layers can negatively impact the overall performance of the DSSC **[33]**.

5.6. Analysis of performance of cells on the basis of resistive parameters:

One of the key factors influencing the overall power conversion efficiency of Dye-Sensitized Solar Cells (DSSCs) is the resistance within the solar cell itself. This resistance can manifest in two distinct forms namely series and shunt resistance, each impacting efficiency for different reasons. These resistances can be calculated from the I-V characteristic curve of the cells **[34]**.

1) Series resistance:

The series resistance results from the sheet resistance of transparent conductive oxide (TCO), the resistance due to improper ionic diffusion in electrolyte, resistance of contacts and the resistance at the interface of counter electrode and electrolyte are the elements responsible for series resistance of DSSC. Ideally series resistance would be zero. Series resistance can be estimated by the slope near the point of Voc on the I-V curve.

2) Shunt Resistance:

Shunt resistance is caused by leakage current through the cell due to impurities or defects in the manufacturing process. Ideally shunt resistance in infinite which means that no additional current path exists. A lower shunt resistance would also lead to a smaller open circuit voltage. Shunt resistance can be calculated by the inverse of slope near the point of short circuit current Isc on the I - V curve.

Hence, the efficiency of dye-sensitized solar cells (DSSCs) is also intricately tied to other parameters, including series resistance (Rs), shunt resistance (Rsh), open-circuit voltage (Voc) and short circuit current (Isc). They are related to recombination as well, which is the factor on which this work is focussed. Optimizing these parameters is essential for enhancing the overall performance of DSSCs.

Carrier recombination and current leakage also leads to resistive losses. These resistive losses are due to series resistance and shunt resistance respectively. Thus, carrier recombination and current leakage limit the performance of DSSCs. The losses are also reflected in the *I–V* curve. The combined resistance on account of materials, electrodes, contacts and interface barriers in photo voltaic cells is commonly referred to as "internal

resistance" (R_i) **[35,36]**. The active layers as well as the supporting layers also contribute to the electrical losses. The series resistance (Rs) lowers J_{sc} and thus affects the fill factor and photo conversion efficiency significantly, although the effect on V_{oc} is minimal. Previous studies have shown that increasing R_s causes a decrease in J_{sc} but has no effect on V_{oc} in a solar cell. The shunt resistance (R_{sh}) is dependent on the device architecture. The factors include charge recombination mechanisms broadly termed as edge effects which result into losses due to active layer pinholes and recombination **[36,37]**. Low shunt resistance (R_{sh}) causes a loss in photo voltage. It also impacts the collection of photocurrent, although to a much lesser extent. This suggests the minimizing of series resistance (Rs) and maximizing of shunt resistance (Rsh) as desirable factors. Hence, structural optimization needs to be undertaken by studying the series and shunt resistances of the fabricated cells.

The method of calculation of series and shunt resistance from I-V graph is given below.

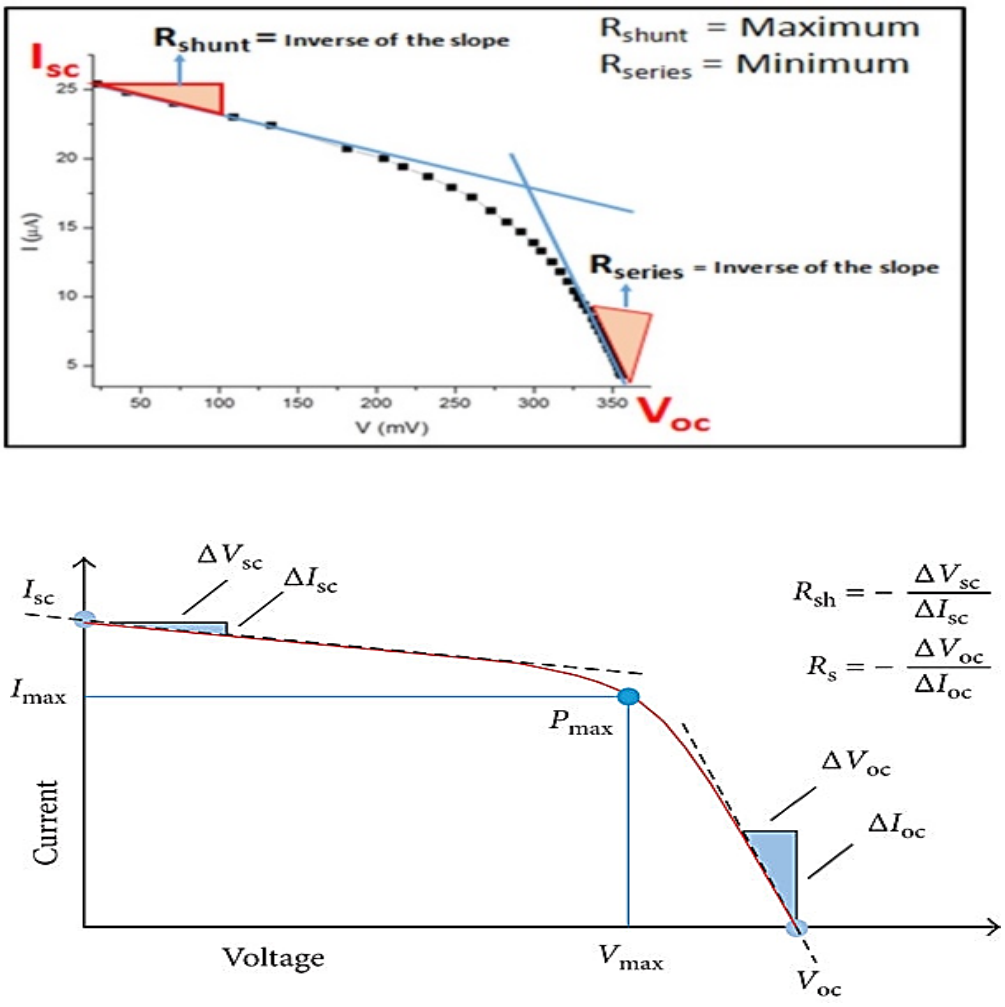

Figure 12: Graphical method for finding Rs and Rsh.

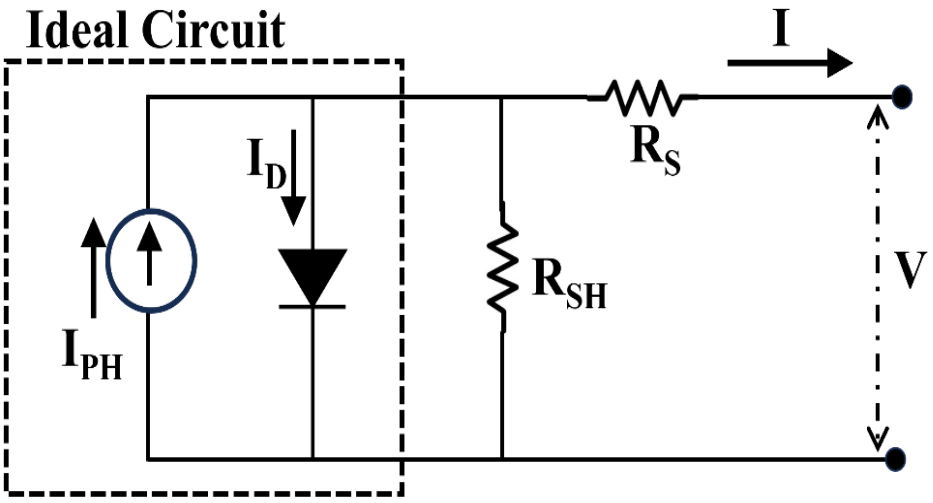

Figure 13: Schematic circuit diagram for Rs and Rsh.

Table 9: Resistance of cells with single layer.

Sample	Thickness (µm)	R_{sh} (Ω)	R_S (Ω)	η %
ZnO	10.45	95.38	17.76	**2.46**
TiO_2	11.34	186.36	11.76	**2.77**
CeO_2	11.56	160.00	171.68	**0.89**
CdS	10.78	114.78	83.36	**0.76**
CuO	10.98	92.82	96.67	**0.35**
ZrO_2	11.34	265.28	175.33	**0.63**

Table 10: Resistance of cells with two layers (ZnO+TiO_2)

Sample	Thickness of ZnO	Thickness of TiO_2 (µm)	R_{sh} (Ω)	R_S (Ω)	η %
ZnO + TiO_2	~2.4 µm	4.86	211.00	28.95	**0.94**
		11.01	219.83	59.89	**1.89**
		12.96	169.08	25.54	**3.90**
		19.80	221.17	25.61	**2.64**

Table 11: Resistance of cells with two layers (ZnO + CeO_2)

Sample	Thickness of ZnO	Thickness of CeO_2 (µm)	R_{sh} (Ω)	R_S (Ω)	η %
ZnO + CeO_2	~2.4 µm	3.24	172.76	5.40	**2.32**
		7.56	159.88	4.29	**3.41**
		11.34	339.39	11.31	**4.25**
		13.45	108.30	20.72	**2.07**

Table 12: Resistance of cells with two layers (ZnO + CdS)

Sample	Thickness of ZnO	Thickness of CdS(µm)	R_{sh} (Ω)	R_S (Ω)	η %
ZnO + CdS	~2.4 µm	4.23	161.88	30.25	**3.90**
		8.23	295.77	89.56	**4.54**
		12.56	151.62	19.84	**5.68**
		15.89	64.62	11.19	**4.55**

Table 13: Resistance of cells with two layers (ZnO + CuO)

Sample	Thickness of ZnO	Thickness of CuO(µm)	R_{sh} (Ω)	R_S (Ω)	η %
ZnO + CuO	~2.4 µm	5.67	170.80	29.41	**0.94**
		8.12	91.43	27.25	**1.21**
		12.89	110.19	23.34	**2.29**
		17.45	159.03	27.08	**1.49**

Table 14: Resistance of cells with two layers (ZnO + ZrO_2)

Sample	Thickness of ZnO	Thickness of ZrO_2(µm)	R_{sh} (Ω)	R_S (Ω)	η %
ZnO + ZrO_2	~2.4 µm	3.78	315.18	13.79	**1.70**
		7.91	450.15	39.85	**1.78**
		12.81	293.45	47.46	**2.07**
		18.23	427.33	21.43	**1.82**

Table 15: Resistance of cells with three layers

Samples	Thickness (µm)	R_{sh} (Ω)	R_S (Ω)	η %
ZnO / TiO_2/ CeO_2	11.89	84.01	12.16	**5.34**
ZnO / TiO_2 /CdS	12.13	148.27	38.10	**4.49**
ZnO / TiO_2 / CuO	11.98	222.69	14.02	**6.42**
ZnO / TiO_2 / ZrO_2	12.78	163.97	8.44	**7.43**
ZnO / CeO_2/ CdS	12.89	119.37	29.17	**5.44**
ZnO / CeO_2/ CuO	12.45	170.66	2.88	**6.44**
ZnO / CeO_2/ ZrO_2	11.67	157.07	10.13	**8.54**
ZnO / CdS / CuO	**12.24**	38.37	6.52	**9.93**
ZnO / CdS / ZrO_2	12.01	69.79	10.78	**8.99**
ZnO / CuO/ ZrO_2	13.45	116.61	15.05	**4.39**

Table 16: Resistance of cells with multiple layers

Sample	Thickness (µm)	R_{sh} (Ω)	R_S (Ω)	η %
ZnO / TiO_2 / CeO_2 / CdS	18.23	586.31	586.31	**0.86**
ZnO / TiO_2 / CeO_2 / CuO	19.67	64.70	64.70	**0.76**
ZnO / TiO_2 / CeO_2 / ZrO_2	19.45	111.93	11.93	**0.71**
ZnO / TiO_2 / CeO_2 / CdS / CuO	22.56	129.96	129.96	**0.69**
ZnO / TiO_2 / CeO_2 / CdS / ZrO_2	22.13	121.02	121.02	**0.64**
ZnO / TiO_2 / CeO_2 / CdS / CuO/ ZrO_2	23.45	108.16	10.816	**0.47**

As mentioned above, the analysis of the cell's performance can be done based on series and shunt resistance.

For the cells with single layer, the highest efficiency was obtained for TiO_2 layer (Table 9). It has a low series resistance and high shunt resistance. This is followed by the cell with ZnO layer, which also has low series resistance. Both TiO_2 and ZnO have proven to be good electrode materials due to their transport properties. The thickness of all the layers is almost similar. The cell with minimum efficiency has moderate values of both series as well as shunt resistance **[38-40]**.

As mentioned above, the two layered cells, with one layer as electrode and the other as barrier, were prepared in sets of four cells for each material combination by varying the thickness of the barrier layer. The results corroborate the findings of earlier studies, which suggest that the optimum thickness is around 12 µm **[41]**.

In case of Zno+TiO_2, the highest efficiency was obtained for thickness of 12.96 µm with low series resistance and relatively high shunt resistance (Table 10). For a similar value of series resistance but higher shunt resistance, the efficiency of another cell was lower. The reason can be attributed to higher thickness (19.8 µm) **[41]**.

For ZnO+CeO_2, the cell with 11.34 µm has a low series resistance and high shunt resistance, giving maximum efficiency in the group (Table 11). The series resistances are quite low for all the cells, while the shunt resistances vary widely.Hence the deciding factor is likely to be the thickness of the barrier layer.

The highest efficiency in the bi-layer cells was observed for the ZnO+CdS combination. The cell with 12.56 µm thickness of CdS barrier layer gives a maximum efficiency of 5.68 %. It has a low series resistance and high shunt resistance (Table 12). The cell with 15.89 µm thickness also gives reasonably good efficiency with a very low series resistance. However a low shunt resistance in this case suggests higher leakage current or fabrication defect. CdS also has a lower optical bandgap which can lead to facilitation of better transport of electrons from dye to barrier layer to electrode.

The combination of ZnO+CuO gives the lowest efficiencies (Table 13). This is also consistent with the result of the single layer cells, where CuO has the lowest efficiency. The series resistance of all the cells in this combination are low while the values of shunt resistance are moderate. However, the UV-Visible absorption characteristics of CuO did not yield distinct absorbance peaks. Hence, the quality of the sample is the most likely reason for the poor performance.

The combination of ZnO+ZrO_2 also yielded low values of efficiencies (Table 14). Here also, the series resistance is on the lower side and shunt resistance high. However the optical band gap of ZrO_2 is very high.

The three layer cells were prepared keeping in view the LUMO levels and hence, the placement of cells was done accordingly. Results are given in Table 15.

ZnO was retained as the electrode layer as in earlier cases.

A. Four cells were prepared with TiO_2 as the first barrier layer, followed by CeO_2, CdS, CuO and ZrO_2 layers respectively.
B. Three cells were prepared with CeO_2 as the first barrier layer, followed by CdS, CuO and ZrO_2 layers respectively.
C. Two cells were prepared with CdS as the first barrier layer, followed by CuO and ZrO_2 layers respectively.
D. One cell was prepared with CuO as the first barrier layer, followed ZrO_2.

This completes the entire sequence.

In the category A, the combination of ZnO / TiO_2 / ZrO_2 gives the highest efficiency of 7.43 %. The series resistance is quite low while the shunt resistance is

higher. The combined thickness of the layers is 12.78 μm. The combination of TiO_2 - ZrO_2 with a predominant role of TiO_2 owing to its better transport properties, seems to be the likely reason for its effective role as inhibitor of recombination.

In the category B, the combination of ZnO / CeO_2/ ZrO_2 gives an efficiency of 8.54%. The series resistance here is also quite low, while the shunt resistance is on the higher side. The thickness is 11.67 μm.

The three layered cells in Category C give the best results, reinforcing the effective role of CdS as a suitable material for barrier layer and its effectiveness as a recombination inhibiting material. The ZnO / CdS / CuO combination gives an efficiency of 9.93 %, which is the highest obtained efficiency. The series resistance is lowest among all cells of three layer combination**[35][36][42]**.

The ZnO / CuO/ ZrO_2 combination fares quite poorly**[36][37]**.

Since the three layer approach was found to yield higher efficiencies, an exercise was undertaken to fabricate cells with multiple layers and investigate their performance. The results are given in Table 16. There is a sharp decline in the efficiencies of the cells. Although the series resistance in some cells are low, their shunt resistance is also on the lower side, suggesting losses due to leakage current. The combined thickness of layers in all these cells is quite high, which is not conducive for better performance.

Thus, optimum thickness and low series resistance emerge as the common factors for better performance. The three layers (one electrode and two barrier layers) yields the best results in terms of efficiency.

5.7. Performance of cells fabricated using electrode layer of composite material:

As evident from the above discussion, the three layer approach gives better results. In this category, one of the combinations that yielded good efficiency is ZnO / TiO_2 / ZrO_2. Hence, a composite of TiO_2 and ZrO_2 was considered to be investigated as a potential electrode or photoanode material. Since TiO_2 is widely used as the material for photoanode, it was appropriate to use it as a reference material for comparison of results. Ti as well as Zr are found to be in the +4 oxidation state in their respective oxides. Besides they have similar ionic radii (0.069 nm and 0,072 nm) respectively. This makes them a widely studied composite material, often with rare earth dopants as activators.

In this study, three samples were synthesized for comparative study. TiO_2, undoped TiO_2 - ZrO_2 and Europium doped TiO_2 - ZrO_2. Europium is one of the most suitable activator and has excellent excitation as well as emission characteristics in the UV – Visible region. It can manifest in +2 as well as +3 states in the composite TiO_2 - ZrO_2 matrix incorporating it into the metallic sites or in an interstitial position. Being a rare earth ion with good shielding effect owing to its 5s 4d electronic configuration, the emission characteristics remain largely unaffected due to the host matrix. Thus, the presence of Eu as dopant can lead to better absorption of solar energy and subsequent emission in the visible region (blue in case of Eu^{+2} and red in case of Eu^{+3}), which would enhance the photo generation of charge carriers and result into higher photo conversion efficiency.

With this in view, samples as mentioned above were synthesized and cells were fabricated using these materials as photoanode layers. Barrier layers were not made, the rationale for which can be explained on the basis of the table given below.

Materials	LUMO energy levels in (eV)
ZnO	**-4.4**
TiO_2	**-4.2**
CeO_2	**-4.1**
CdS	**-4.0**
CuO	**-3.8**
ZrO_2	**-3.5**
Dye (Anthocyanin)	**-2.93**

The barrier layers require proper placement in consistence with the LUMO energy levels. The composite material is a combination of TiO_2 and ZrO_2, which are placed at the two ends of the sequence, as given in the above table. Hence, taking any material as barrier layer, which is between the two, would lead to a mismatch of LUMO levels between the barrier and electrode layer.

As in all other cases, Ruthenium Dye and Platinum were replaced by Pomegranate juice and graphite coating respectively.

The I-V curves are given in Figure. 14. The photovoltaic parameters are given in Table 17. The efficiency increases in the ascending order from the cell fabricated using TiO_2 followed by undoped TiO_2-ZrO_2 and Eu doped TiO_2-ZrO_2. The highest efficiency of 6.25 % has been obtained for the cell made by using Eu doped TiO_2-ZrO_2. The doping of Eu increases the Anatase phase content of TiO_2, which is the most effective phase of TiO_2 for DSSC operation. The decrease in crystallite size of the doped material (6.47 nm) also improves the performance, which can be attributed to increase in surface area on account of lower crystallite size that results into higher amount of dye being adsorbed on the film **[43, 44]**.

The increased efficiency can be attributed to the introduction of additional energy levels, which increases the conduction electron density in Eu doped TiO_2-ZrO_2 layer **[45-47]**. All the cells mentioned above have very low series resistance and low shunt resistance as well. While the low series resistance is desirable, the lower values of shunt resistance indicate fabrication issues and thus provide opportunity for improvement.

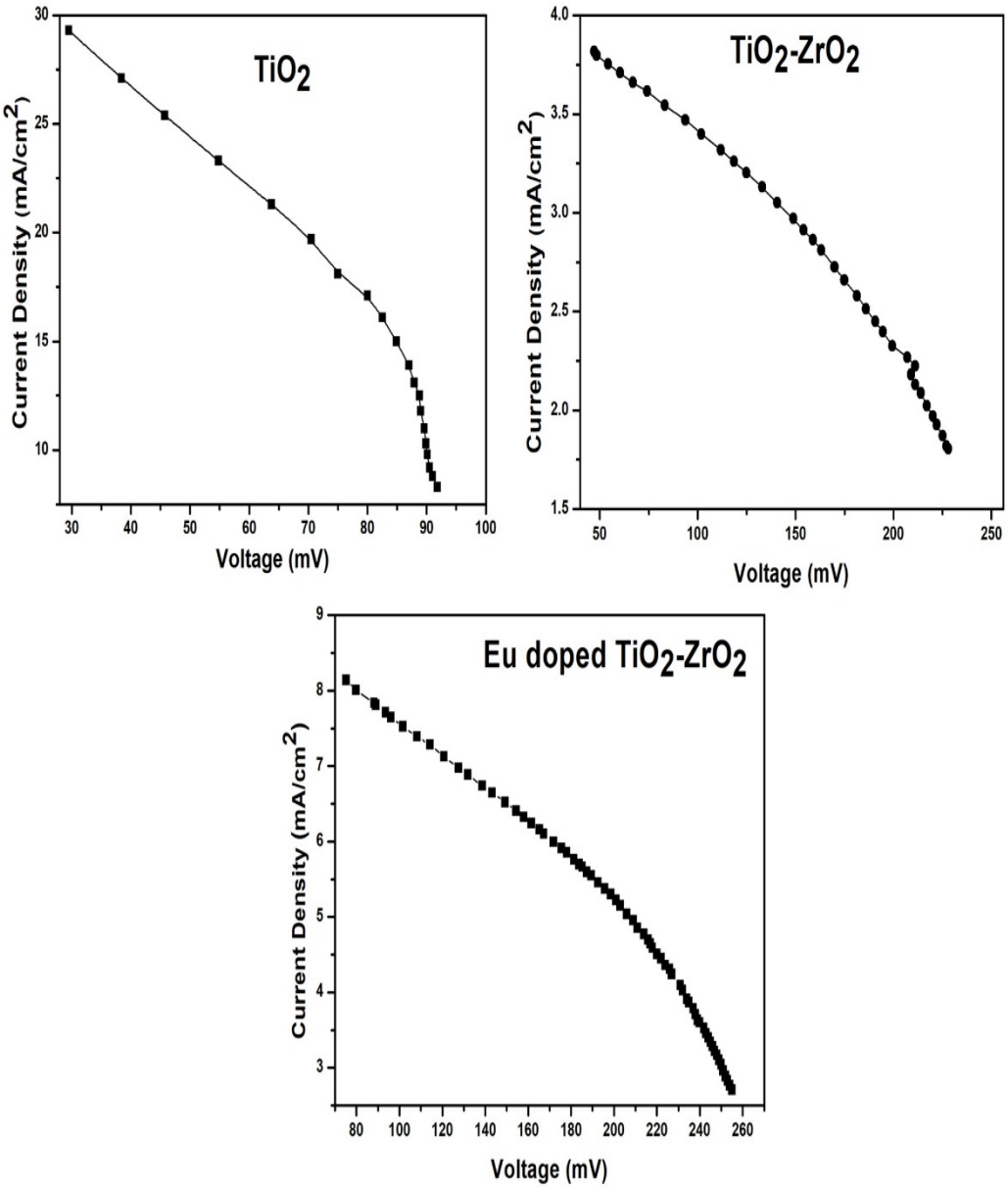

Figure14: I-V curves of cells.

Table 17: Photovoltaic parameters.

Sample	Jsc (mA/cm^2)	Voc (mV)	FF	R_{sh} (Ω)	R_S (Ω)	η %
TiO_2	8.7	200	0.061	40.00	4.5	**0.71**
TiO_2-ZrO_2	3.1	377	0.256	98.00	3.6	**1.97**
Eu doped TiO_2-ZrO_2	8.1	373	0.312	36.00	1.2	**6.25**

Reference:

1. Diamant, Y., Chappel, S., Chen, S. G., Melamed, O., & Zaban, A. (2004). Core–shell nanoporous electrode for dye sensitized solar cells: the effect of shell characteristics on the electronic properties of the electrode. *Coordination Chemistry Reviews, 248*(13-14), 1271-1276.
2. Lin, C., Tsai, F. Y., Lee, M. H., Lee, C. H., Tien, T. C., Wang, L. P., & Tsai, S. Y. (2009). Enhanced performance of dye-sensitized solar cells by an Al2O3 charge-recombination barrier formed by low-temperature atomic layer deposition. *Journal of Materials Chemistry, 19*(19), 2999-3003.
3. Dyartanti, E. R., Sunaryati, N., Alhakim, R. R., Putri, L. N., Putri, A. Y. M., Nurohmah, A. R., & Nisa, S. S. (2021, March). Recent Development of Polyvinylidene Fluoride/Cellulose Membranes Electrolyte Separator for Lithium Ion Batteries. In *IOP Conference Series: Materials Science and Engineering(Vol. 1096, No. 1, p. 012144)*. IOP Publishing.
4. GOODSHIP, V. Bethany MIDDLETON a Ruth CHERRINGTON. *Design and manufacture of plastic components for multifunctionality: structural composites, injection molding, and 3D printing*.
5. Khoo, H. E., Azlan, A., Tang, S. T., & Lim, S. M. (2017). Anthocyanidins and anthocyanins: Colored pigments as food, pharmaceutical ingredients, and the potential health benefits. *Food & nutrition research*.
6. Harborne, J. B., & Williams, C. A. (2001). Anthocyanins and other flavonoids. *Natural product reports, 18*(3), 310-333.
7. Trouillas, P., Sancho-García, J. C., De Freitas, V., Gierschner, J., Otyepka, M., & Dangles, O. (2016). Stabilizing and modulating color by copigmentation: Insights from theory and experiment. *Chemical reviews, 116*(9), 4937-4982.
8. Choi, H., Han, J., Kang, M. S., Song, K., & Ko, J. (2014). Aqueous electrolytes-based dye-sensitized solar cells using I−/I3− redox couple to achieve ≥ 4% power conversion efficiency. *Bull. Korean Chem. Soc, 35*(5), 1433-1439.
9. Grätzel, M., & Moser, J. E. (2001). Solar energy conversion. *Electron transfer in chemistry, 5*(3), 589-644.
10. Sun, Y., Gao, Y., Hu, J., Liu, C., Sui, Y., Lv, S., ... & Yang, L. (2020). Comparison of effects of ZnO and TiO2 compact layer on performance of perovskite solar cells. *Journal of Solid State Chemistry, 287*, 121387.

11. Chou, T. P., Zhang, Q., Russo, B., Fryxell, G. E., & Cao, G. (2007). Titania particle size effect on the overall performance of dye-sensitized solar cells. *The Journal of Physical Chemistry C, 111*(17), 6296-6302.
12. Sherly, E. D., Vijaya, J. J., Kennedy, L. J., Meenakshisundaram, A., & Lavanya, M. (2016). A comparative study of the effects of CuO, NiO, ZrO2 and CeO2 coupling on the photocatalytic activity and characteristics of ZnO. *Korean Journal of Chemical Engineering, 33*, 1431-1440.
13. Hossain, S. S., Tarek, M., Munusamy, T. D., Karim, K. M. R., Roopan, S. M., Sarkar, S. M., ... & Khan, M. M. R. (2020). Facile synthesis of CuO/CdS heterostructure photocatalyst for the effective degradation of dye under visible light. *Environmental Research, 188*, 109803.
14. Iwamoto, S., Sazanami, Y., Inoue, M., Inoue, T., Hoshi, T., Shigaki, K., ... & Maenosono, A. (2008). Fabrication of Dye-Sensitized Solar Cells with an Open-Circuit Photovoltage of 1 V. *ChemSusChem: Chemistry & Sustainability Energy & Materials, 1*(5), 401-403.
15. Ni, M., Leung, M. K., Leung, D. Y., & Sumathy, K. (2006). Theoretical modeling of TiO2/TCO interfacial effect on dye-sensitized solar cell performance. *Solar Energy Materials and Solar Cells, 90*(13), 2000-2009.
16. Mondal, B. K., Mostaque, S. K., & Hossain, J. (2022). Theoretical insights into a high-efficiency Sb2Se3-based dual-heterojunction solar cell. *Heliyon, 8*(3).
17. Liao, J. F., Wu, W. Q., Jiang, Y., Zhong, J. X., Wang, L., & Kuang, D. B. (2020). Understanding of carrier dynamics, heterojunction merits and device physics: towards designing efficient carrier transport layer-free perovskite solar cells. *Chemical Society Reviews, 49*(2), 354-381.
18. Sulaeman, U., & Abdullah, A. Z. (2017). The way forward for the modification of dye-sensitized solar cell towards better power conversion efficiency. *Renewable and Sustainable Energy Reviews, 74*, 438-452.
19. Sengupta, D., Das, P., Mondal, B., & Mukherjee, K. (2016). Effects of doping, morphology and film-thickness of photo-anode materials for dye sensitized solar cell application–A review. *Renewable and Sustainable Energy Reviews, 60*, 356-376.
20. Taleb, A., Mesguich, F., Hérissan, A., Colbeau-Justin, C., Yanpeng, X., & Dubot, P. (2016). Optimized TiO2 nanoparticle packing for DSSC photovoltaic applications. *Solar Energy Materials and Solar Cells, 148*, 52-59

21. Hosni, M., Kusumawati, Y., Farhat, S., Jouini, N., & Pauporte, T. (2014). Effects of oxide nanoparticle size and shape on electronic structure, charge transport, and recombination in dye-sensitized solar cell photoelectrodes. The Journal of Physical Chemistry C, 118(30), 16791-16798.
22. Son, S., Hwang, S. H., Kim, C., Yun, J. Y., & Jang, J. (2013). Designed synthesis of SiO2/TiO2 core/shell structure as light scattering material for highly efficient dye-sensitized solar cells. ACS applied materials & interfaces, 5(11), 4815-4820.
23. Abrari, M., Ahmadi, M., Chenari, H. M., & Ghanaatshoar, M. (2024). Investigating the effect of ZrO2 nanofibers in ZnO-based photoanodes to increase dye-sensitized solar cells (DSSC) efficiency: Inspecting the porosity and charge transfer properties in ZnO/ZrO2 nanocomposite photoanode. Optical Materials, 147, 114690.
24. Zhou, Y., Xia, C., Hu, X., Huang, W., Aref, A. A., Wang, B., ... & Tang, Y. (2014). Dye-sensitized solar cells based on nanoparticle-decorated ZnO/SnO2 core/shell nanoneedle arrays. Applied surface science, 292, 111-116.
25. Hamadanian, M., & Jabbari, V. (2011). Investigation on the energy conversion of dye-sensitized solar cells based on TiO 2 core/shell using metal oxide as a barrier layer. Applied Solar Energy, 47, 281-288.
26. Arka, G. N., Prasad, S. B., & Singh, S. (2021). Comprehensive study on dye sensitized solar cell in subsystem level to excel performance potential: A review. Solar Energy, 226, 192-213.
27. Selopal, G. S., Memarian, N., Milan, R., Concina, I., Sberveglieri, G., & Vomiero, A. (2014). Effect of blocking layer to boost photoconversion efficiency in ZnO dye-sensitized solar cells. ACS Applied Materials & Interfaces, 6(14), 11236-11244.
28. Alberti, A., Pellegrino, G., Condorelli, G. G., Bongiorno, C., Morita, S., La Magna, A., & Miyasaka, T. (2014). Efficiency enhancement in ZnO: Al-based dye-sensitized solar cells structured with sputtered TiO2 blocking layers. The Journal of Physical Chemistry C, 118(13), 6576-6585.
29. Hardin, B. E., Hoke, E. T., Armstrong, P. B., Yum, J. H., Comte, P., Torres, T., ... & McGehee, M. D. (2009). Increased light harvesting in dye-sensitized solar cells with energy relay dyes. Nature photonics, 3(7), 406-411.

30. Manjceevan, A., & Bandara, J. (2018). Systematic stacking of PbS/CdS/CdSe multi-layered quantum dots for the enhancement of solar cell efficiency by harvesting wide solar spectrum. Electrochimica Acta, 271, 567-575
31. Fathima, M. I., & Wilson, K. J. (2019). Role of multilayer antireflective coating in ZnO based dye sensitized solar cell. *Vacuum, 165*, 58-61.
32. Khan, M. I., Farooq, W. A., Saleem, M., Bhatti, K. A., Atif, M., & Hanif, A. (2019). Phase change, band gap energy and electrical resistivity of Mg doped TiO2 multilayer thin films for dye sensitized solar cells applications. *Ceramics International, 45*(17), 21436-21439.
33. Meng, S., & Kaxiras, E. (2010). Electron and hole dynamics in dye-sensitized solar cells: influencing factors and systematic trends. *Nano letters, 10*(4), 1238-1247.
34. Nowsherwan, G. A., Iqbal, M. A., Rehman, S. U., Zaib, A., Sadiq, M. I., Dogar, M. A., & Choi, J. R. (2023). Numerical optimization and performance evaluation of ZnPC: PC70BM based dye-sensitized solar cell. *Scientific reports, 13*(1), 10431.
35. Tvingstedt, K., Gil-Escrig, L., Momblona, C., Rieder, P., Kiermasch, D., Sessolo, M., ... & Dyakonov, V. (2017). Removing leakage and surface recombination in planar perovskite solar cells. *ACS Energy Letters, 2*(2), 424-430.
36. Singh, R., Sandhu, S., & Lee, J. J. (2019). Elucidating the effect of shunt losses on the performance of mesoporous perovskite solar cells. *Solar Energy, 193*, 956-961.
37. Karthick, S., Velumani, S., & Bouclé, J. (2020). Experimental and SCAPS simulated formamidinium perovskite solar cells: A comparison of device performance. *Solar Energy, 205*, 349-357.
38. Chandiran, A. K., Abdi-Jalebi, M., Nazeeruddin, M. K., & Grätzel, M. (2014). Analysis of electron transfer properties of ZnO and TiO2 photoanodes for dye-sensitized solar cells. *ACS nano, 8*(3), 2261-2268.
39. Hernández, S., Hidalgo, D., Sacco, A., Chiodoni, A., Lamberti, A., Cauda, V., ... & Saracco, G. (2015). Comparison of photocatalytic and transport properties of TiO 2 and ZnO nanostructures for solar-driven water splitting. *Physical Chemistry Chemical Physics, 17*(12), 7775-7786.

40. Quintana, M., Edvinsson, T., Hagfeldt, A., & Boschloo, G. (2007). Comparison of dye-sensitized ZnO and TiO2 solar cells: studies of charge transport and carrier lifetime. *The Journal of Physical Chemistry C, 111*(2), 1035-1041.
41. Lin, C. Y., Lai, Y. H., Chen, H. W., Chen, J. G., Kung, C. W., Vittal, L. R., & Ho, K. C. (2011). Highly efficient dye-sensitized solar cell with a ZnO nanosheet-based photoanode. Energy & Environmental Science, 4(9), 3448-3455.
42. Sheikh, M. S., Roy, A., Dutta, A., Sundaram, S., Mallick, T. K., & Sinha, T. P. (2021). Nanostructured perovskite oxides for dye-sensitized solar cells. Journal of Physics D: Applied Physics, 54(49), 493001.
43. Zhang, Q., & Cao, G. (2013). U.S. Patent No. 8,558,107. Washington, DC: U.S. Patent and Trademark Office.
44. Tomar, L., Bhatt, P., Desai, R., & Chakrabarty, B. (2022). Enhanced Efficiency of Dye Sensitized Solar Cell Using Eu Doped TiO2-ZrO2 Nanocomposite. Recent Patents on Nanotechnology, 16(4), 333-338.
45. Mendes, A. M. M., Mendes, J. G. M., Aguilar, H. I. P. D. C., Gratzel, M., Andrade, L. M. M., Gonçalves, L. F. M., & Da Costa, C. A. V. (2013). U.S. Patent No. 8,567,110. Washington, DC: U.S. Patent and Trademark Office.
46. Gibson, E., Feldt, S., & Gabrielsson, E. (2013). U.S. Patent Application No. 13/805,137.
47. Lee, J. J., Evans, D. R., Nishimura, K. Y., Vail, S. A., & Pan, W. (2012). U.S. Patent Application No. 12/892,779.